Analytica Chimica Acta xxx (2018) 1–9

Contents lists available at ScienceDirect

Analytica Chimica Acta

journal homepage: www.elsevier.com/locate/aca

Graphene blended with SnO_2 and Pd-Pt nanocages for sensitive non-enzymatic electrochemical detection of H_2O_2 released from living cells

Yamin Fu, Di Huang, Congming Li, Lina Zou**, Baoxian Ye*

College of Chemistry and Molecular Engineering, Zhengzhou University, Zhengzhou 450001, PR China

HIGHLIGHTS

- Graphene blended with SnO_2 and PdPd nanocages composite was synthesized.
- Pd-Pt nanocages and SnO_2/graphene nanosheets modified electrode (PdPt NCs@SGN/GCE) has high sensitivity for the determination of hydrogen peroxide (H_2O_2).
- The constructed biosensor provided to be reliable for determination of H_2O_2 secreted from human cervical cancer cells (Hela cells).

GRAPHICAL ABSTRACT

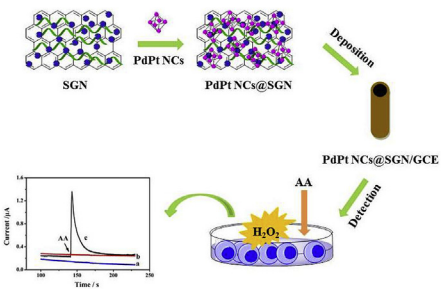

ARTICLE INFO

Article history:
Received 6 November 2017
Received in revised form
23 January 2018
Accepted 25 January 2018
Available online xxx

Keywords:
Hydrogen peroxide
SnO_2
Pd-Pt nanocages
Hela cell
Electrochemistry

ABSTRACT

This paper described a novel, facile and nonenzymatic electrochemical biosensor to detect hydrogen peroxide (H_2O_2). The sensor was fabricated based on Pd-Pt nanocages and SnO_2/graphene nanosheets modified electrode (PdPt NCs@SGN/GCE). The electrochemical behavior of PdPt NCs@SGN/GCE exhibited excellent catalytic activity toward H_2O_2 with fast response, high selectivity, superior sensitivity, low detection limit of 0.3 μM and large linear range from 1 μM to 300 μM. Under these obvious advantages, the constructed biosensor provided to be reliable for determination of H_2O_2 secreted from human cervical cancer cells (Hela cells). Hence, the proposed biosensor is a promising candidate for detection of H_2O_2 in situ released from living cells in clinical diagnostics.

1. Introduction

Hydrogen peroxide (H_2O_2) is an ordinary product of oxygen metabolism of cells. In the cell, non-normal level of H_2O_2 was demonstrated to bring about apoptosis, carcinogenesis and to cause some chronic diseases such as aging, infarction, atherosclerosis, heart attack and cancer [1–5]. Therefore, it is a matter of cardinal significance to monitor the concentration of H_2O_2 under physiological conditions [6–10]. Up to now, various analytical techniques, such as spectrophotometry [11,12], chromatography [13] and electrochemistry [14–16] have been accepted for the determination of H_2O_2. Among these techniques, electrochemical method, a more suitable method of determination in situ and real-time, has attained more attention based on their fast response, high sensitivity and good selectivity. In the field of electrochemistry, enzyme-based H_2O_2 biosensors have been widely used due to their specificity and high sensitivity [17–20]. Nonetheless, the intrinsic

* Corresponding author.
** Corresponding author.
E-mail address: yebx@zzu.edu.cn (B. Ye).

https://doi.org/10.1016/j.aca.2018.01.067
0003-2670/

shortages limited its application, including high cost, environmental instability, complicated immobilization procedure and denaturation [21]. In order to overcome these problems, non-enzymatic H_2O_2 biosensors have been explored and achieved intense interest by scientists.

In the construction of non-enzymatic H_2O_2 biosensors, enzymes have usually been replaced by nanomaterials with electrocatalytic activity toward H_2O_2, such as noble metals (Pt, Pd, Ag, and Au) [22–25], their alloys (PdPt, AgCu) [26,27] and metal oxide (CuO, Co_3O_4, Fe_3O_4) [28–30]. Among the noble metal catalysts, PdPt alloy nanoparticles (NPs) are well-known with high catalytic activity of H_2O_2 compared to the single Pd or Pt NPs [26]. Besides the component of NPs, size and shape also play a nonnegligible function on their catalytic performance. Hollow metallic nanospheres, possessed the larger surface area, were provided with the more excellent catalytic effect compared to their solid counterparts [31–36]. In addition, they can reduce the dosage of rare and expensive noble metals. However, the research based on PdPt nanocages (PdPt NCs) for H_2O_2 sensor is narrow. Therefore, PdPt NCs was presented as a catalytic material for detecting H_2O_2 in this work.

In the practical application, carbon materials have been widely used as supporters to load the catalysts, which can effectively avoid the aggregate of metal nanoparticles [37–39]. Graphene (GR) is one of the most popular candidates. GR could enhance the catalytic activity due to its outstanding properties such as high electrical conductivity, large surface area, high stability and wide potential window [40,41]. However, GR sheets are easy to stack during the synthesis process. Decorate nanoparticles on the GR not only improve the stability and dispersion of nanoparticles, but also reduce the GR stacking.

In view of the above consideration, SnO_2/graphene nanosheets (SGN) were synthesized as a supporter, and then the prepared PdPt NCs was decorated with it. Finally, the resultant graphene nanocomposites were used as new electrode materials to construct an enzyme-free biosensor for the detection of H_2O_2. There are mainly two reasons for choosing SnO_2 to modified graphene. Firstly, previous work reported that SnO_2/graphene composites showed good catalytic activity in the reduction of H_2O_2 [42]. Secondly, compared to noble metals, SnO_2 possess advantages of low cost, abundant and environmental friendly. Owing to the synergy effect of the SGN and PdPt NCs, this novel nonenzymatic H_2O_2 biosensor showed significantly improved electrocatalytic activity toward H_2O_2 compared with the SGN/GCE and Pd@SGN/GCE. Excellent properties like low detection limit, wide linear range, outstanding stability, reproducibility and selectivity make it possible for reliable detection of H_2O_2 released from live HeLa cancer cells (Scheme 1). Moreover, evaluate the intracellular H_2O_2 concentration is potentially valuable for physiological and pathological H_2O_2 monitoring.

2. Experimental

2.1. Material and apparatus

Graphite flakes (Sigma-Aldrich, St.Louis, Missouri, USA), poly (diallyldimethylammonium chloride) (PDDA, 35 wt.% in water, average Mw ≤ 100,000, Aladdin Chemistry Co., Ltd., Shanghai, China), stannic chloride dehydrate ($SnCl_2 \cdot H_2O$, ≥98%, Shanghai Yuanye Biological Technology Co., Ltd., Shanghai, China), potassium tetrachloropalladate (II) (K_2PdCl_4, 99%, J&K Scientific Co., Ltd., Beijing, China), potassium tetrachloroplatinate(II) (K_2PtCl_4, 99.95%, J&K Scientific Co., Ltd., Beijing, China), potassium bromide (KBr, 99.0%, Aladdin Chemistry Co., Ltd., Shanghai, China), L-Ascorbic acid (AA, 99%, J&K Scientific Co., Ltd., Beijing, China), Polyvinylpyrrolidone (PVP, Mw≅58000, Aladdin Chemistry Co., Ltd., Shanghai, China), Citrate (CA, ≥99.5%, Aladdin Chemistry Co., Ltd., Shanghai, China) and Hydrogen peroxide (H_2O_2, 30%, Tianjin fuchen chemical reagents factory, Tianjin, China) were all used as received without any further purification.

The surface morphology figures were acquired using a JEOL-2100 EX transmission electron microscope (TEM). The elementary composition was obtained with EDAX APOLLO-X energy dispersive X-ray analysis. Powder X-ray diffraction (XRD) analysis was performed with a X-ray diffractometer conducted by Cu Ka radiation source (λ = 1.54056 Å). UV–visible spectroscopy was carried out on a Lambda 35 UV–vis spectrometer (Pgeneral General Instrument) with samples in a quartz cuvette operated from 200 to 800 nm. Electrochemical measurements were performed on a RST 3000 electrochemical workstation (Zhengzhou Shiruisi Instrument Technology Co. Ltd., China.). A conventional three-electrode cell was employed with a platinum wire counter electrode, a saturated calomel reference electrode (SCE) and bare or modified glassy carbon working electrode (4 mm in diameter). All the water used in this work was acquired from a Thermo Scientific Barnstead GenPure water purification system (Shanghai, China) with electrical resistance ≥18.2 MΩ·cm.

2.2. Synthesis of SGN nanosheets

SGN nanosheets were prepared by one-step hydrothermal method as previously reported [43]. Herein, $SnCl_2 \cdot H_2O$ is not only a reducing agent for graphene oxide (GO), but also a precursor of SnO_2. PDDA was used to improve the dispersion of GO, which will be benefit for the growth of SnO_2. Briefly, GO was synthesized by the Hummer's method [44] and 20 mL of GO solution (0.5 mg mL^{-1}) was ultrasonicated for 3h until forming a homogeneous suspension. Subsequently, 400 μL of PDDA solution (35%) was injected into the GO suspension under the vigorously stirring. After 0.5 h, 0.6 g of $SnCl_2 \cdot H_2O$ and 150 μL of HCl were added in the mixture. Next, the reaction was refluxed at 90 °C for 3 h. Finally, the product was centrifuged, washed with ultrapure water for several times and dried under vacuum at 65 °C.

2.3. Synthesis of PdPt NCs@SGN composites

Firstly, PVP (80 mg), AA (40 mg) and KBr (400 mg) was placed in 8.0 mL ultrapure water and preheated to 80 °C in an oil bath for 10 min. After that, 3.0 mL of K_2PdCl_4 (50 mg) solution was added. The reaction was refluxed at 80 °C for 3 h. Finally, Pd nanocubes were collected by centrifugation, washed three times with water and redispersed in 11 mL of water.

7 mL of an aqueous solution containing PVP (30 mg), KBr (280 mg), and CA (280 mg) was placed in a round-bottom flask. Subsequently, 1 mL of the aqueous suspension of Pd nanocubes was added to the flask and heated to 90 °C under magnetic stirring. Meanwhile, 3 mL of the aqueous solution containing 28 mg K_2PtCl_4 was added to the flask and the mixture was refluxed at 90 °C for 12 h. Finally, the solution was centrifuged, washed three times with water and redispersed in 8 mL of water [45].

SGN composite (5 mg) was injected into 5 mL of the aqueous suspension of PdPt NCs. The mixture was ultrasonicated 2 h to form PdPt NCs@SGN nanocomposites. For comparison, Pd@SGN composites were synthesized by the similar way.

2.4. Fabrication of H_2O_2 sensor

Prior to modification, the glassy carbon electrode (GCE) was polished to a mirror-like smoothness with aqueous slurries, rinsed with deionized water and then ultra-sonicated in absolutely ethanol for a few minutes before air-drying at room temperature.

Please cite this article in press as: Y. Fu, et al., Graphene blended with SnO_2 and Pd-Pt nanocages for sensitive non-enzymatic electrochemical detection of H_2O_2 released from living cells, Analytica Chimica Acta (2018), https://doi.org/10.1016/j.aca.2018.01.067

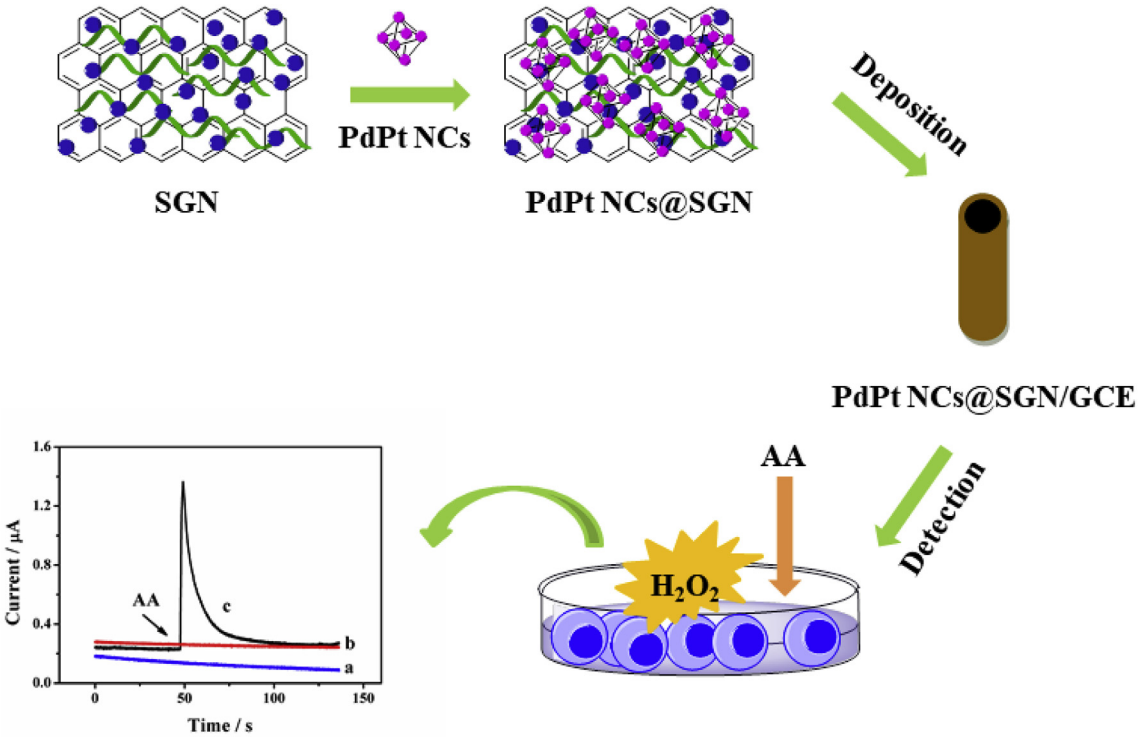

Scheme 1. Schematic of the PdPt NCs@SGN/GCE used for detecting H_2O_2 released from Hela cells.

Next, the modified electrode was obtained by depositing 10 μL of PdPt NCs@SGN suspension on the electrode surface and drying under room temperature. The desired modified electrode was obtained and denoted as PdPt NCs@SGN/GCE. For comparison, Pd@SGN/GCE was fabricated from the similar procedure.

2.5. Cell culture

Hela cells (Hematology, Chinese Academy of Medical Sciences), belonged to human cervical cancer cell lines, were used in this study. The Hela cells were cultured at 37 °C with 5% CO_2 in a 95% humid atmosphere with DMEM (high glucose, Gibco) containing 10% heat-inactivated fetal calf serum (Sigma-Aldrich, St. Louis, MO, USA), 100 U/mL penicillin (Sigma-Aldrich), and 100 mg mL^{-1} streptomycin (Sigma-Aldrich).

2.6. Electrochemical detection of H_2O_2 released by cell

Hela cells grown in 12.25 cm^2 cell culture flasks (1.0×10^6 cells) for electrochemical experiments. Cell number was estimated by a cell counter. The culture media was removed and the cells were washed three times with PBS buffer (pH 7.4, 0.01 M), and then 2 mL PBS buffer (pH 7.4, 0.1 M) was added for real sample measurements. Before the measurement, the supernatant liquid of cells was deoxygenated with nitrogen slowly. The amperometric detection of the release flux of H_2O_2 from Hela cells was performed using the PdPt NCs@SGN/GCE at −0.1 V (vs. SCE). Ascorbic acid (AA) was injected into the cells suspension, which can motivate cells generation of H_2O_2.

3. Results and discussion

3.1. Characterization of nanocomposite

UV−vis absorption spectra diagram was proposed to analyze that the GO was reduced to graphene. In Fig. 1A, curve a, GO showed a strong adsorption peak at 230 nm on account of the π to π* transition of aromatic C−C bond. The adsorption peak (260 nm) of SGN in curve b indicated the complete reduction of GO to graphene [46].

Fig. 1B showed XRD patterns of GO (a) and SGN (b). In curve a, the peak (001, $2\theta = 10.4°$) was the reflection of GO. From curve b, diffraction peaks at110, 101, 211 and 310 ($2\theta = 25.52°$, 34.16°, 51.37°, 62.27°) were consistent with the standard XRD data for the tetragonal rutile like SnO_2 phase (JCPDS no. 41−1445) [47], indicating that SnO_2 has been synthesized in this composite. Compared to curve a, the peak of 001 ($2\theta = 10.4°$) disappeared in curve b display the reduction of GO. Moreover, the lack of distinct peaks belonging to GR might be due to the overlap at the high (110) peak of SnO_2 and the low weight ratio of GR in the composite. The XRD patterns of PdPt NCs were showed in Fig. 1C. The diffraction peaks of PdPt NCs at approximately 40°, 47°, 68° and 81° are attributed to 111, 200, 220 and 311 planes of FCC structure of PdPt. Because Pt and Pd possess the same crystal structure (FCC) and very close lattice parameter, the sets of diffraction peak at Pt and Pd are overlapped [48]. The unmarked peak in Fig. 1C belonged the monocrystaline silicon chip which was the substrate.

X-ray photoelectron spectroscopy (XPS) was conducted to study the surface composition of PdPt NCs@SGN. The XPS spectrum was shown in Fig. S1 in which five main elements including C, O, Sn, Pd and Pt can be distinguished. From the Sn 3d spectrum, the two symmetrical peaks at 492.5 and 484.2 eV can be ascribed to 3d 3/2 and 3d 5/2 of Sn (IV), respectively, suggesting the existence of Sn^{4+} in the product. Thus, the peak of both Pd 3d and Pt 4f can be separated to Pd $3d_{5/2}$, Pd $3d_{3/2}$, Pt $4f_{7/2}$ and Pt $4f_{5/2}$ suggesting the successful decoration of PdPt NCs in composite. It should be noted that the peak of the oxygenated functional groups (C=O, O=C-O) weren't observed in C 1s indicating the efficient reduction of GO and the formation of rGO in PdPt NCs@SGN. These results were consistent with the information in XRD.

Please cite this article in press as: Y. Fu, et al., Graphene blended with SnO_2 and Pd-Pt nanocages for sensitive non-enzymatic electrochemical detection of H_2O_2 released from living cells, Analytica Chimica Acta (2018), https://doi.org/10.1016/j.aca.2018.01.067

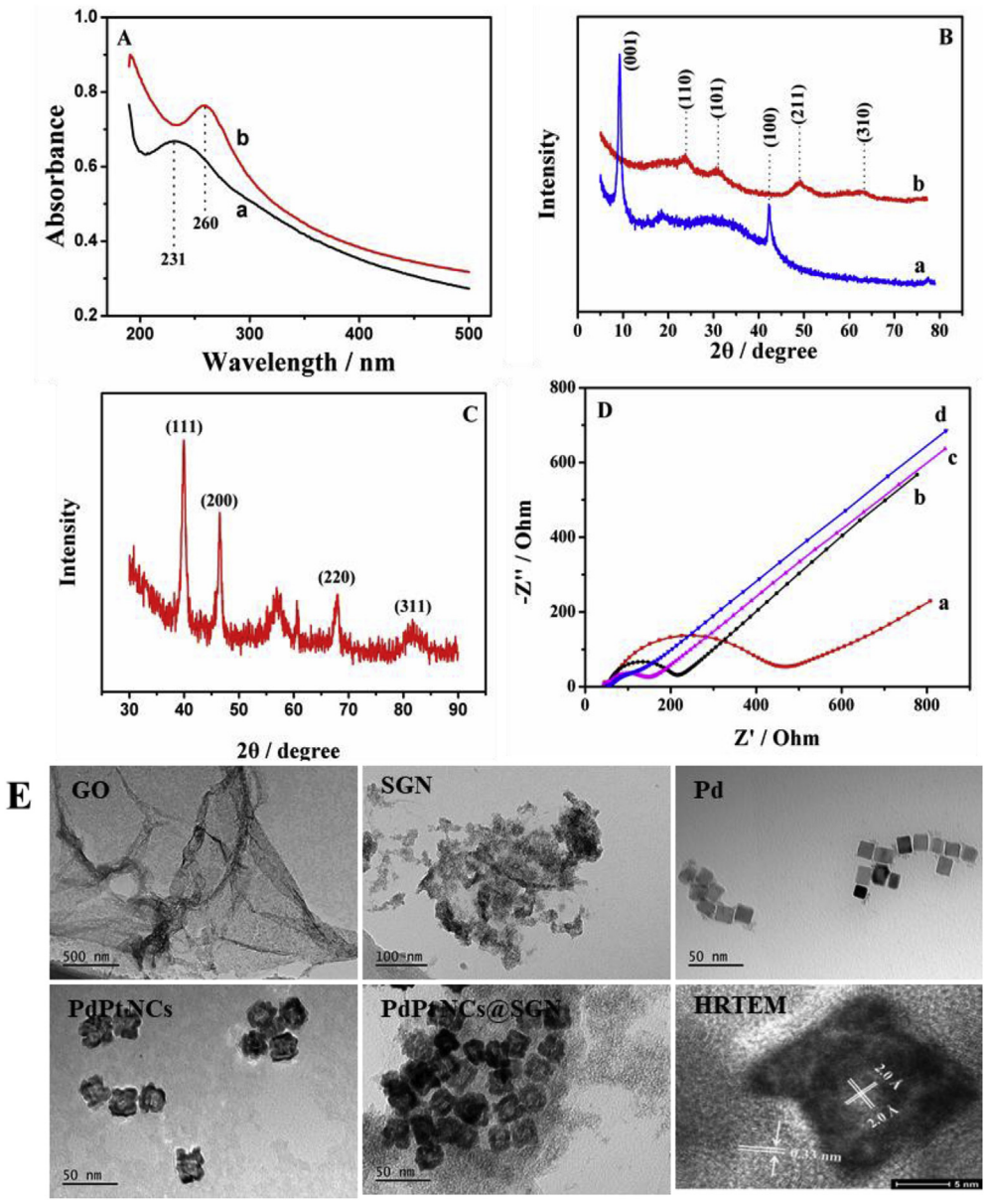

Fig. 1. (A) UV–vis absorption spectra of GO (a) and SGN (b). (B) XRD patterns of GO (a), SGN (b). (C) XRD patterns of PdPt NCs. (D) Nyquist plots obtained at GCE (a), SGN/GCE (b), Pd@SGN/GCE (c) and PdPt NCs@SGN/GCE (d). Supporting electrolyte: 5×10^{-3} mol L^{-1} $Fe(CN)_6^{3-/4-}$ (1:1) with 0.1 mol L^{-1} KCl solution; Working potential: 0.285 V; Frequency: 1 M Hz to 0.01 Hz. (E) TEM images of GO, SGN, Pd nanocubes, PbPt NCs, PdPt NCs@SGN composite and HRTEM image.

Fig. 1E showed TEM images of GO, SGN, Pd nanocubes, PdPt NCs and PdPt NCs@SGN composite. In Fig. 1E, GO was layered and plicate, which like a piece of gauze. However, the surface morphology of SGN composite presented flaky. Pd showed a shape of cube, called Pd nanocubes. PdPt NCs showed a hollow cage structures with an average length of 22 nm. The well dispersed PdPt NCs on SGN was also clearly in Fig. 1E, which composed the desired nanocomposite. Additionally, the high-resolution TEM (HRTEM) image revealed that the whole SGN sheet was loaded with SnO_2 and decorated with PdPt NCs. The distance of the visible lattice fringes over a large area was measured to be 0.33 nm, corresponding to the d-spacing of (110) planes of SnO_2. Besides, the fringes with lattice sapcing of 2.0 Å can be indexed to the (200) planes of a FCC lattice in PdPt NCs.

The element distribution of PdPt NCs@SGN was measured by EDS mapping (see Fig. S2), which clearly presented the support component elements of C, O, Sn, Pd and Pt. The element mapping in C, Sn, O, Pd and Pt in Fig. S2 revealed that the PdPt NCs distributed on the surface of SGN uniformly, which was consistent with the TEM image of PdPt NCs@SGN.

3.2. The electrochemical characterization of proposed sensor

As an effective method of monitoring the interfacial properties of the modified electrodes, electrochemical impedance spectroscope (EIS) was putting forward. Fig. 1D recorded the Nyquist plots of redox probes $[Fe(CN)_6]^{3-/4-}$ at GCE (a), SGN/GCE (b), Pd@SGN/GCE (c) and PdPt NCs@SGN/GCE (d) respectively. In the impedance spectra, the lower frequencies of the linear section were attributed to the diffusion-limited process. The higher frequencies of the semicircle portion were related to the charge-transfer limited process. The value of changer-transfer resistance (R_{ct}) is

Please cite this article in press as: Y. Fu, et al., Graphene blended with SnO_2 and Pd-Pt nanocages for sensitive non-enzymatic electrochemical detection of H_2O_2 released from living cells, Analytica Chimica Acta (2018), https://doi.org/10.1016/j.aca.2018.01.067

proportional to the semicircle diameter. It is known that a smaller semicircle means a higher electron transfer rate and vice versa. As the Fig. 1D shown, after the GCE was decorated with the SGN (b), Rct was decreased based on the good conductivity and positive charges of the SGN, which was helpful in the electron transfers of the redox probes on the electrode surface. Upon modification of GCE with the Pd@SGN (c), Rct was further decreased owing to the improved conductivity of Pd nanocubes. When the Pd nanocubes were changed by PdPt NCs, PdPt NCs@SGN/GCE (d) obtained the smallest Rct. The result once again proved that PdPt NCs has better conductivity compared to Pd nanocubes. In generally, the highest electron transfer efficiency was obtained from the PdPt NCs@SGN/GCE. Such excellent conductivity resulted from the synergistic effects of PdPt NCs and SGN. This result illustrated that PdPt NCs@SGN possessed a great potential to develop non-enzymatic sensitive electrochemical sensor.

3.3. The electrochemical behavior of H_2O_2 at the PdPt NCs/SGN/GCE

The H_2O_2 sensing experiments was completed by cyclic voltammetry in 0.1 M PBS (pH 7.4) buffer. Fig. 2 showed the CVs of blank PBS (red line) and 0.5 mM H_2O_2 at bare GCE (A), SGN/GCE (B), Pd@SGN/GCE (C) and PdPt NCs@SGN/GCE (D) respectively. All experiments were performed in N_2-saturated PBS buffer. In the absence of H_2O_2, no reduction peak was observed at GCE (A) while small reduction peaks were observed on SGN/GCE (B), Pd@SGN/GCE (C) and PdPt NCs@SGN/GCE (D) in the potential range of the −0.6 ~ +0.6 V respectively, which might be attributed to the reduction of SnO_2 and Pd. In the presence of 0.5 mM H_2O_2, a weak reduction peak of H_2O_2 was observed on SGN/GCE. However on the Pd@SGN/GCE, the reduction peak current of H_2O_2 was enhanced obviously at more positive reduction potential, which showed pronounced electrocatalytic properties. Compared with the above two, PdPt NCs@SGN/GCE exhibited stronger electrocatalytic response. Such excellent electrocatalytic property can be owing to two factors: First, based on the high surface areas and high electronic conductivity, PdPt NCs and SGN both have electrocatalytic activity to H_2O_2. Second, as a superior support with good dispersity, SGN can load more PdPt NCs and prevent aggregation effectively to maximize the available surface area, which can increase the active sites to increase the catalytic activity.

The electrochemical responses of H_2O_2 at different modified electrodes were also investigated by potentiostatic electrolysis. Fig. 2E showed the amperometric response I-t curves obtained at GCE (a), SGN/GCE (b), Pd@SGN/GCE (c) and PdPt NCs@SGN/GCE (d) by successive addition of H_2O_2 (0.5 mM) into continuously stirred PBS buffer at a working potential of −0.1 V. Compared to other electrodes, PdPt NCs@SGN/GCE exhibited a maximum increase in amperometric current upon the successive addition of 0.5 mM H_2O_2, which also presented that the PdPt NCs@SGN/GCE significantly enhanced the electrocatalytic activity. On the basis of the results described above, the PdPt NCs@SGN/GCE can effectively catalyze the reduction of H_2O_2 and used in quantitative detection of H_2O_2 is feasible.

3.4. Influence of pH and scan rate

The effect of pH was investigated to achieve a superior view of the reaction process in 0.1 M PBS containing 0.5 mM H_2O_2. Fig. 3A was the voltammetric stacking graphs over a pH range of 4.5−8.5. With the pH of supporting electrolyte increased, the response current of H_2O_2 was raised. In Fig. 3B, the response current increased slowly when pH reached to 7.4. Moreover, pH 7.4 provided a possibility for biological applications and it was selected as the optimum pH value of H_2O_2 detection.

In order to study the charge transport characteristics of the PdPt NCs@SGN nanocomposite film, voltammetric curves with changing scan rates (0.01, 0.02, 0.04, 0.06, 0.08, 0.10, 0.15, 0.20, 0.25 V s^{-1}) were recorded and shown in Fig. 4. The cathodic peak currents (Ip) increased linearly with the square root of scan rate (v) enhancement (Inset in Fig. 4). The linear relationship between Ip (μA) and $v^{1/2}$ (mV s^{-1}) $^{1/2}$ was expressed as following equation (Fig. 8B): Ip

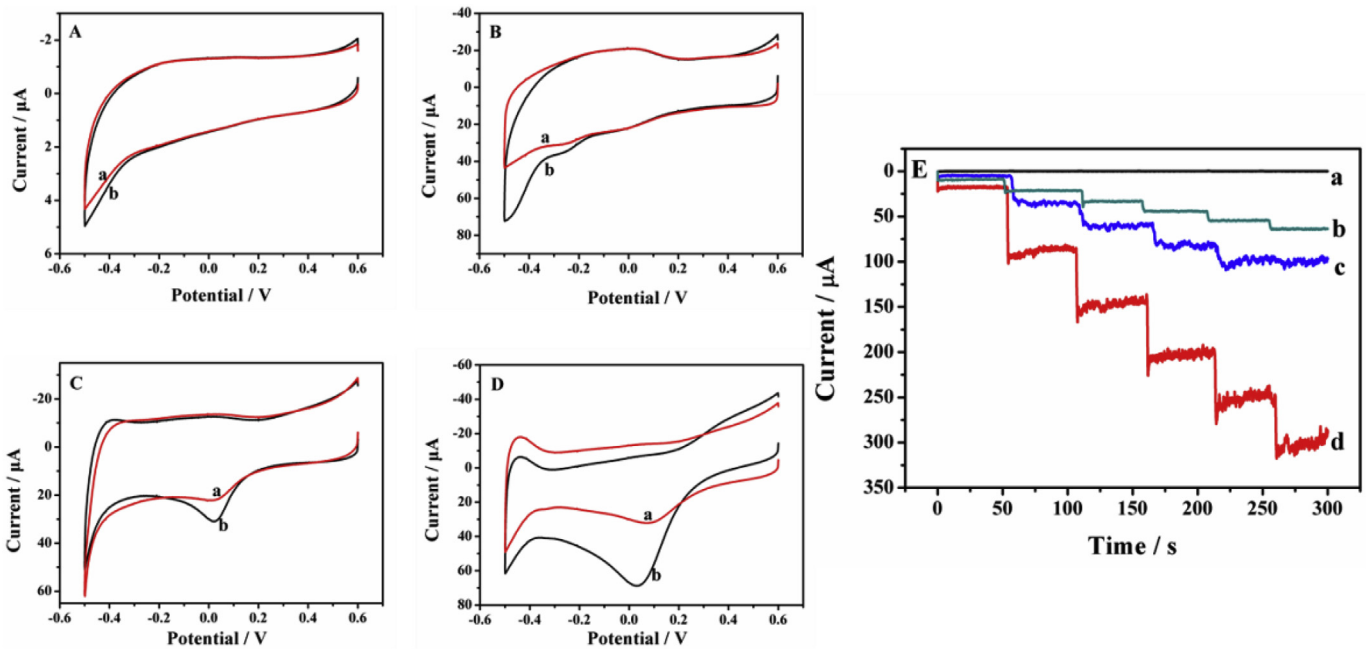

Fig. 2. CVs of the GCE (A), SGN (B), Pd@SGN (C) and PdPt NCs@SGN (D) in the absence (red) and presence (black) of 0.5 mM H_2O_2 in 0.1 M pH 7.4 PBS at 0.10 V s^{-1}. (E) Amperometric i−t curves of GCE (a), SGN@GCE (b), Pd@SGN/GCE (c) and PdPt NCs@SGN/GCE (d) in N_2-saturated PBS (0.1 M, pH 7.4) at - 0.1 V with successive addition of H_2O_2. (For interpretation of the references to colour in this figure legend, the reader is referred to the Web version of this article.)

Please cite this article in press as: Y. Fu, et al., Graphene blended with SnO_2 and Pd-Pt nanocages for sensitive non-enzymatic electrochemical detection of H_2O_2 released from living cells, Analytica Chimica Acta (2018), https://doi.org/10.1016/j.aca.2018.01.067

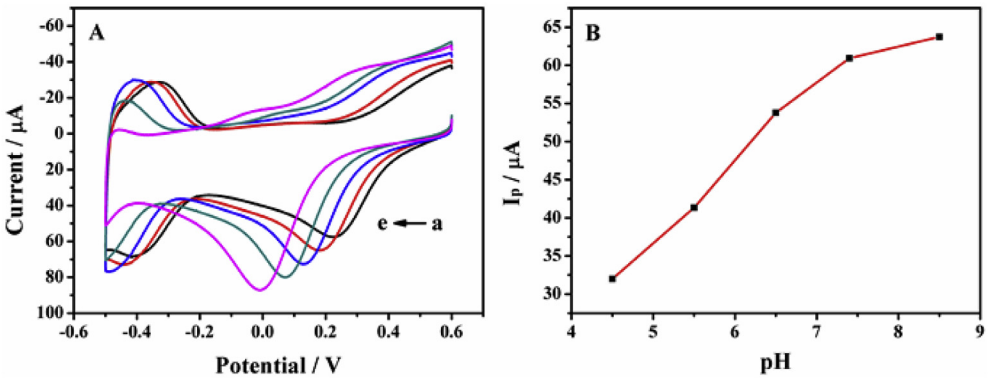

Fig. 3. (A) CVs of PdPt NCs@SGN/GCE in 0.5 mM H_2O_2 with different pH (a–e:4.5, 5.5, 6.5, 7.4, 8.5). (B) The relationship between the peak current and pH. Scan rate 0.1 V s^{-1}.

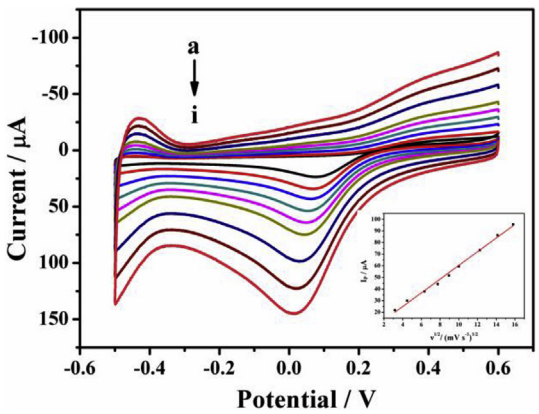

Fig. 4. CVs of PdPt NCs@SGN/GCE in 0.5 mM H_2O_2 (pH 7.4) with the scan rates from 10 to 250 mV s^{-1}. (Inset: Ip versus $v^{1/2}$).

(μA) = 5.88 $v^{1/2}$ (mV s^{-1}) $^{1/2}$ + 1.46 (R^2 = 0.994), which demonstrated that the reduction process of H_2O_2 at the prepared PdPt NCs@SGN/GCE was a diffusion-confined process.

3.5. Amperometric response to H_2O_2 detection

Amperometric method was adopted in order to frame a sensitive assay. Fig. 5A displayed I-t curves recorded from PdPt NCs@SGN/GCE for H_2O_2 detection at −0.1 V in 0.1 M PBS (pH 7.4). The inset of Fig. 5A exhibits the I-t response of low content concentration of H_2O_2 at PdPt NCs@SGN/GCE. Every time the H_2O_2 was added, the current rapidly reached steady-state within 3s. The reduction currents of were linearly increased with the concentrations of H_2O_2. The linear equation is I (μA) = 0.2395C (μM) + 0.9088 (R^2 = 0.997). A relevant linear relationship was established in the range of 1 μM–300 μM and the limit of detection (LOD) was calculated to be 0.3 μM (S/N = 3). A comparison of linear range, LOD and sensitivity for PdPt NCs@SGN/GCE with other H_2O_2 sensors reported are shown in Table 1 [49–56].

As one of the most important analytical factors, anti-interference ability must be discussed. Some electroactive species were studied by the amperometric method in PBS. Fig. 6 displayed that there was no obvious current response after addition of AA, UA, glucose, leucine and DA. Therefore, it was no influence on the detection of H_2O_2 in the presence of these electroactive species, indicating the sensor had an excellent selectivity.

The reproducibility and stability was also being evaluated. Five determinations using the same sensor (Fig. 7B), the relative standard deviation (RSD) of response currents was of 2.3%, which indicated a nice repeatability. Moreover, the RSD of five independently sensors was 4.1% for five independent determination (Fig. 7A), indicating superior reproducibility of the sensor preparation and good stability of the electrode material. The current was only changed 3.3% after storage of a sensor for two weeks. Therefore, the sensor possessed an excellent repeatability and nice stability, exhibited a wide potential application.

3.6. In vitro biological sample analysis

The practical application of the PdPt NCs@SGN/GCE was utilized by measuring the concentration of H_2O_2 in human serum. First, the

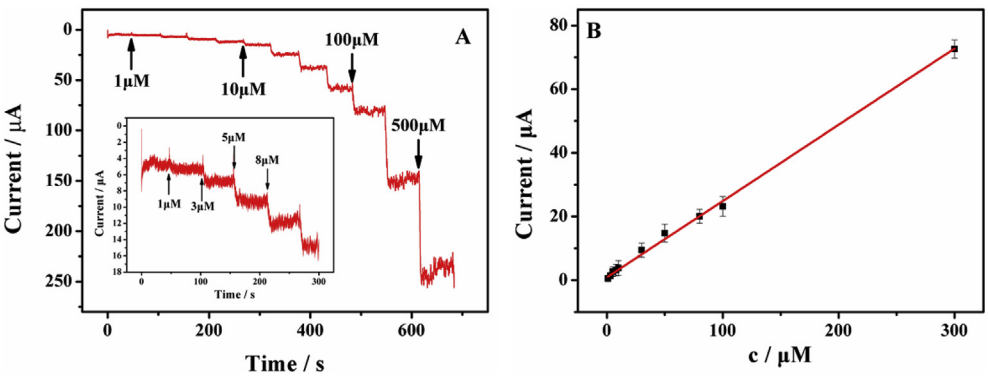

Fig. 5. (A) Amperometric response of the PdPt NCs@SGN/GCE with successive addition of different concentrations of H_2O_2 at the potential of −0.1 V. (Inset: a partial magnification of the current response in the low concentration of H_2O_2 solution). (B) The corresponding calibration curve for H_2O_2 sensing.

Please cite this article in press as: Y. Fu, et al., Graphene blended with SnO_2 and Pd-Pt nanocages for sensitive non-enzymatic electrochemical detection of H_2O_2 released from living cells, Analytica Chimica Acta (2018), https://doi.org/10.1016/j.aca.2018.01.067

Table 1
Comparison of the performance of various H_2O_2 sensors.

Materials	Linear range (μM)	LOD (μM)	Sensitivity (μA mM^{-1} cm^{-2})	Reference
Pt nanowire	5–3000	9.6	1360000	[49]
MnO_2/graphene	100–45400	10	59	[50]
MoS_2/Pt NPs	1–100	0.686	–	[51]
SnO_2-PEI-Gr	9–1640	1.0	–	[42]
Ag NP/rGO	100–10000	3.6	–	[53]
Pd nanocubes	100–24000	7.5	287.7	[54]
Ag-Fe_2O_3-rGO	1.6–57000	0.5	50.8	[55]
AgY	10–500	1.4	650.7	[56]
Ag/Na-ZSM-5	30–140	2.5	71	[57]
PdPt NCs@SGN	1–300	0.3	14968750	This work

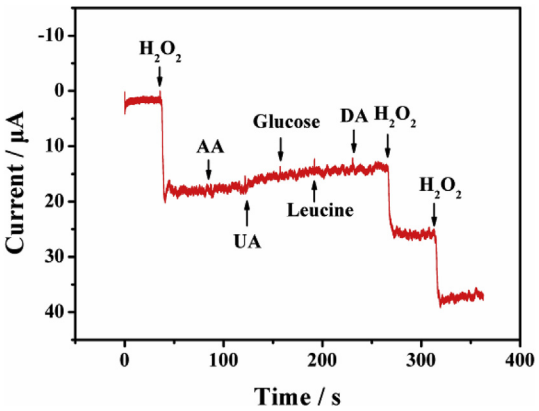

Fig. 6. Amperometric response to successive addition of 0.1 mM H_2O_2, 0.2 mM AA, 0.2 mM UA, 0.5 mM glucose, 0.2 mM Leucine and a second 0.1 mM H_2O_2 of PdPt NCs@SGN/GCE at −0.1 V in 0.1 M PBS 7.4.

serum was diluted 20 times. Next, amperometric method was selected to detect the practical samples in PBS. No any current response when a certain amount of serum injected into the cell. To testify the feasibility of the biosensor in serum, the recovery measurements were carried out for the determination of H_2O_2. The detection results listed in Table 2 showed an excellent reliability in practical application as the recoveries were range of 98.94% to 104.18%.

In cells, non-normal level of H_2O_2 was associated with some chronic diseases like cancer [3]. In general, H_2O_2 holds a low physiological concentration relatively under the normal levels.

Table 2
Recovery detection for H_2O_2 in Human Serum.

Sample	Found(μM)	Added(μM)	After added (μM)	RSD(%)	Mean recovery(%)
serum	0				
		75.00	77.21	1.9	102.81
		75.00	78.29	1.2	104.18
		75.00	74.16	2.3	98.94

*Average value of three replicate measurements.

However, it will increase rapidly once the cells were stimulated [57]. Ascorbic acid (AA) can disturb the redox process of cells, hence it can motivate cells to generate large number of H_2O_2 [58].

To explore the practical application of the as-prepared PdPt NCs@SGN/GCE, the H_2O_2 released from living cells was monitored by this biosensor. On the basis of interference experiment, AA was no response at the biosensor. So AA was explored as the stimulant to excite the Hela cells generating amounts of H_2O_2 in a short time. Fig. 8 was the amperimetric response curves of H_2O_2 in PBS (pH 7.4) at −0.1 V. In curve a, there was no response when 10 μM AA was injected into the PBS, indicating the AA was no response at the biosensor. When 10 μM AA was added into the PBS containing Hela cells, a significant response was received (curve c), which demonstrated the H_2O_2 was released from Hela cells by stimulating with AA. If some catalase (300 U/mL) was existed in solution, the response signal of H_2O_2 would disappear (curve b), because the catalase decomposed H_2O_2 fleetly.

The peak current was about 1.36 μA in curve c, corresponding to 1.88 μM H_2O_2 which was consistent with the published report [59]. Thus, the flux of H_2O_2 were calculated to be 376 ± 23 amol $cell^{-1}$ s^{-1}

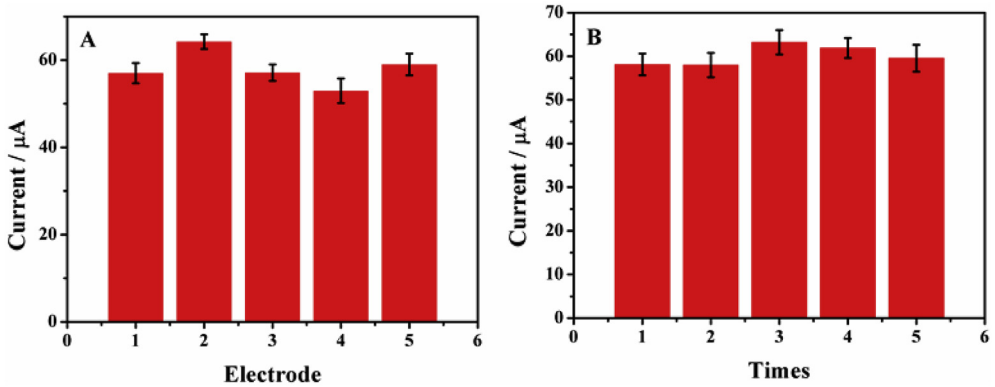

Fig. 7. (A) Current responses of five different sensors in 0.5 mM H_2O_2. (B) Current responses of one sensor for five individual determination in 0.5 mM H_2O_2.

Please cite this article in press as: Y. Fu, et al., Graphene blended with SnO_2 and Pd-Pt nanocages for sensitive non-enzymatic electrochemical detection of H_2O_2 released from living cells, Analytica Chimica Acta (2018), https://doi.org/10.1016/j.aca.2018.01.067

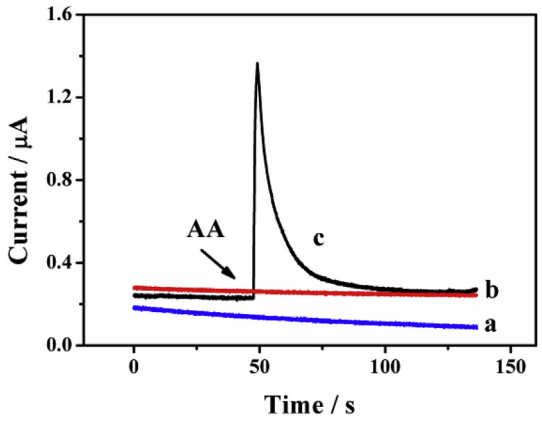

Fig. 8. Amperometric response of H_2O_2 released from Hela cells stimulated by AA at −0.1 V in PBS. (a)PBS; (b) 1×10^6 Hela cells and 300U/mL catalases in PBS; (c) 1×10^6 Hela cells in PBS.

according to the literature [60]. In consequence, this biosensor possessed a potential application for detecting H_2O_2 released from living cells.

4. Conclusions

In conclusion, the work presented facile synthesis of PdPt NCs@SGN nanocomposite, and used in constructing a sensitive non-enzymatic H_2O_2 sensor. The synergistic effects of the PdPt NCs and SGN enable the sensor to exhibit high electrocatalytic activity and excellent selectivity to the detection of H_2O_2. Moreover, the sensor has other excellent characteristics: lower detection limit, superior sensitivity and rapid response. These integrated features guaranteed the reliable in situ detection of H_2O_2 secreted by live HeLa cells.

Acknowledgements

This work was supported by the National Natural Science Foundation of China (Grant no. 21575130; U1504216) and Startup Research Fund of Zhengzhou University (Grant no. 1511316006).

Appendix A. Supplementary data

Supplementary data related to this article can be found at https://doi.org/10.1016/j.aca.2018.01.067.

References

[1] M. Hayyan, M.A. Hashim, I.M. AlNashef, Superoxide ion: generation and chemical implications, Chem. Rev. 116 (2016) 3029–3085.
[2] G. Fang, C. Liu, Y. Wang, D.D. Dionysiou, D. Zhou, Photogeneration of reactive oxygen species from biochar suspension for diethyl phthalate degradation, Appl. Catal., B 214 (2017) 34–45.
[3] T.P. Devasagayam, J.C. Tilak, K.K. Boloor, K.S. Sane, S.S. Ghaskadbi, Free radicals and antioxidants in human health: current status and future prospects, J. Assoc. Phys. India 52 (2004) 34–35.
[4] H. Ohshima, M. Tatemichi, T. Sawa, Chemical basis of inflammation-induced carcinogenesis, Arch. Biochem. Biophys. 417 (2003) 3–11.
[5] D.E. Handy, J. Loscalzo, Responses to reductive stress in the cardiovascular system, Free Radical Biol. Med. 109 (2017) 114–124.
[6] W. Maruyama, et al., N-methyl(R)salsolinol produces hydroxyl radicals: involvement to neurotoxicity, Free Radical Biol. Med. 19 (1995) 67–75.
[7] C. Amatore, S. Arbault, D. Bruce, P.D. Oliveira, Characterization of the electrochemical oxidation of peroxynitrite: relevance to oxidative stress bursts measured at the single cell level, Chemistry 7 (2001) 4171–4179.
[8] E.W. Miller, A.E. Albers, Boronate-based fluorescent probes for imaging cellular hydrogen peroxide, J. Am. Chem. Soc. 127 (2005) 16652–16659.
[9] Y. Zhang, X. Bai, X. Wang, K.K. Shiu, Y. Zhu, Highly sensitive graphene-Pt nanocomposites amperometric biosensor and its application in living cell H_2O_2 detection, Anal. Chem. 86 (2014) 9459–9465.
[10] V.S. Khodade, M. Sharath Chandra, A. Banerjee, S. Lahiri, M. Pulipeta, R. Rangarajan, H. Chakrapani, Bioreductively activated reactive oxygen species (ROS) generators as MRSA inhibitors, ACS Med. Chem. Lett. 5 (2014) 777–781.
[11] D. Li, M. Wang, N. Cheng, X. Xue, L. Wu, W. Cao, A modified FOX-1 method for Micro-determination of hydrogen peroxide in honey samples, Food Chem. 237 (2017) 225–231.
[12] S. Goyen, M. Pernice, M. Szabó, M.E. Warner, P.J. Ralph, D.J. Suggett, A molecular physiology basis for functional diversity of hydrogen peroxide production amongst Symbiodinium spp, Mar. Biol. 164 (2017) 46.
[13] Y.J. Guo, L.Q. Sun, B.Y. Yu, J. Qi, An integrated antioxidant activity fingerprint for commercial teas based on their capacities to scavenge reactive oxygen species, Food Chem. 237 (2017) 645–653.
[14] H. Dai, W. Lu, X. Zuo, Q. Zhu, C. Pan, X. Niu, J. Liu, H. Chen, X. Chen, A novel biosensor based on boronic acid functionalized metal-organic frameworks for the determination of hydrogen peroxide released from living cells, Biosens. Bioelectron. 95 (2017) 131–137.
[15] S. Chatterjee, A. Chen, Functionalization of carbon buckypaper for the sensitive determination of hydrogen peroxide in human urine, Biosens. Bioelectron. 35 (2012) 302–307.
[16] J. Bai, X. Jiang, A facile one-pot synthesis of copper sulfide-decorated reduced graphene oxide composites for enhanced detecting of H_2O_2 in biological environments, Anal. Chem. 85 (2013) 8095–8101.
[17] X. Chen, C. Fu, Y. Wang, W. Yang, D.G. Evans, Direct electrochemistry and electrocatalysis based on a film of horseradish peroxidase intercalated into Ni-Al layered double hydroxide nanosheets, Biosens. Bioelectron. 24 (2008) 356–361.
[18] C.Y. Liu, J.M. Hu, Hydrogen peroxide biosensor based on the direct electrochemistry of myoglobin immobilized on silver nanoparticles doped carbon nanotubes film, Biosens. Bioelectron. 24 (2009) 2149–2154.
[19] S. Dramińska, R. Bilewicz, Bienzymatic mediatorless sensing of total hydrogen peroxide with catalase and multi-copper enzyme co-adsorbed at carbon nanotube-modified electrodes, Sens. Actuators, B 248 (2017) 493–499.
[20] Z. Liu, B. Zhao, Y. Shi, C. Guo, H. Yang, Z. Li, Novel nonenzymatic hydrogen peroxide sensor based on iron oxide-silver hybrid submicrospheres, Talanta 81 (2010) 1650–1654.
[21] E. Shoji, M.S. Freund, Potentiometric sensors based on the inductive effect on the pK(a) of poly(aniline): a nonenzymatic glucose sensor, J. Am. Chem. Soc. 123 (2001) 3383–3384.
[22] L. Wu, W. Yin, X. Tan, P. Wang, F. Ding, H. Zhang, B. Wang, W. Zhang, H. Han, Direct reduction of HAuCl 4 for the visual detection of intracellular hydrogen peroxide based on Au-Pt/SiO2 nanospheres, Sens. Actuators, B 248 (2017) 367–373.
[23] J. Xi, Y. Zhang, N. Wang, L. Wang, Z. Zhang, F. Xiao, S. Wang, Ultrafine Pd nanoparticles encapsulated in microporous Co3O4 hollow nanospheres for in situ molecular detection of living cells, ACS Appl. Mater. Interfaces 7 (2015) 5583–5590.
[24] Y. Liu, X. Liu, Z. Guo, Z. Hu, Z. Xue, X. Lu, Horseradish peroxidase supported on porous graphene as a novel sensing platform for detection of hydrogen peroxide in living cells sensitively, Biosens. Bioelectron. 87 (2017) 101–107.
[25] J. Liu, X. Bo, Z. Zhao, L. Guo, Highly exposed Pt nanoparticles supported on porous graphene for electrochemical detection of hydrogen peroxide in living cells, Biosens. Bioelectron. 74 (2015) 71–77.
[26] S.G. Lee, G.C. Kim, H.C. Choi, Preparation of bimetallic Pd-Pt nanoparticles supported on carbon nanotubes for enhanced electrocatalytic H2O2 detection, Bull. Kor. Chem. Soc. 36 (2015) 1309–1310.
[27] K. Kang, F. Chen, Preparation of Ag–Cu bimetallic dendritic nanostructures and their hydrogen peroxide electroreduction property, J. Appl. Electrochem. 43 (2013) 667–677.
[28] L. Zhang, X. Hai, C. Xia, X.-W. Chen, J.-H. Wang, Growth of CuO nanoneedles on graphene quantum dots as peroxidase mimics for sensitive colorimetric detection of hydrogen peroxide and glucose, Sens. Actuators, B 248 (2017) 374–384.
[29] T. Zhang, C. He, F. Sun, Y. Ding, M. Wang, L. Peng, J. Wang, Y. Lin, Co3O4 nanoparticles anchored on nitrogen-doped reduced graphene oxide as a multifunctional catalyst for H2O2 reduction, oxygen reduction and evolution reaction, Sci. Rep. 7 (2017), 43638.
[30] M. Asif, H. Liu, A. Aziz, H. Wang, Z. Wang, M. Ajmal, F. Xiao, H. Liu, Core-shell iron oxide-layered double hydroxide: high electrochemical sensing performance of H2O2 biomarker in live cancer cells with plasma therapeutics, Biosens. Bioelectron. 97 (2017) 352–359.
[31] Na Li, et al., An ultrasensitive electrochemical immunosensor for CEA using MWCNT-NH2 supported PdPt nanocages as labels for signal amplification, J. Mater. Chem. B 3 (2015) 2006–2011.
[32] X. Xiao, S.S. Zheng, X.R. Li, G.X. Zhang, X.T. Guo, Facile synthesis of ultrathin Ni-MOF nanobelts for high-efficiency determination of glucose in human serum, J. Mater. Chem. B 5 (2017) 5234–5239.
[33] S.S. Zheng, X.R. Li, B.Y. Yan, Q. Hu, X. Xiao, H.G. Xue, H. Pang, Transition-metal (Fe, Co, Ni) based metal-organic frameworks for electrochemical energy storage, Adv. Energy Mater. 7 (2017), 1602733.
[34] X. Xiao, X.R. Li, S.S. Zheng, J.Y. Shao, H.G. Xue, H. Pang, Nanostructured germanium anode materials for advanced rechargeable batteries, Adv. Mater. Interfaces 4 (2017), 1600798.
[35] X.R. Li, H.G. Xue, H. Pang, Facile synthesis and shape evolution of well-defined phosphotungstic acid potassium nanocrystals as a highly efficient visible-

light-driven photocatalyst, Nanoscale 9 (2016) 216–222.
[36] X.R. Li, S.Y. Ding, X. Xiao, J.Y. Shao, J.L. Wei, H. Pang, Y. Yu, N, S co-doped 3D mesoporous carbon–$Co_3Si_2O_5(OH)_4$ architectures for high-performance flexible pseudo-solid-state supercapacitors, J. Mater. Chem. 5 (2017), 12774.
[37] Y. Zhang, X. Bai, X. Wang, K.K. Shiu, Y. Zhu, H. Jiang, An ultrasensitive electrochemical immunosensor for CEA using MWCNT-NH2 supported PdPt nanocages as labels for signal amplification, Anal. Chem. 86 (2014) 9459–9465.
[38] Jian Liu, et al., Highly exposed Pt nanoparticles supported on porous graphene for electrochemical detection of hydrogen peroxide in living cells, Biosens. Bioelectron. 74 (2015) 71–77.
[39] R.M. Félix-Navarro, M. Beltrán-Gastélum, M.I. Salazar-Gastélum, C. Silva-Carrillo, E.A. Reynoso-Soto, S. Pérez-Sicairos, S.W. Lin, F. Paraguay-Delgado, G. Alonso-Núñez, Pt–Pd bimetallic nanoparticles on MWCNTs: catalyst for hydrogen peroxide electrosynthesis, J. Nanopart. Res. 15 (2013).
[40] K.S. Novoselov, et al., Electric field effect in atomically thin carbon films, Science 306 (2004) 666.
[41] C. Wu, Q. Cheng, K. Wu, G. Wu, Q. Li, Graphene prepared by one-pot solvent exfoliation as a highly sensitive platform for electrochemical sensing, Anal. Chim. Acta 825 (2014) 26–33.
[42] Y. Liu, L. Wang, L. Yang, Y. Zhan, L. Zou, B. Ye, Nonenzymatic H2O2 electrochemical sensor based on SnO2-NPs coated polyethylenimine functionalized graphene, Electroanalysis 29 (2017) 2044–2052.
[43] Y. Fu, L. Wang, Y. Duan, L. Zou, B. Ye, Facile synthesized SnO2 decorated functionalized graphene modified electrode for sensitive determination of daidzein, Talanta 168 (2017) 1–9.
[44] S. William, Hummers, R.E. Offeman, Preparation of graphitic oxide, J. Am. Chem. Soc. 80 (1958) 1339.
[45] Hui Zhang, et al., Facile synthesis of Pd–Pt alloy nanocages and their enhanced performance for preferential oxidation of CO in excess hydrogen, ACS Nano 5 (2011) 8212–8222.
[46] J. Shen, Y. Hu, C. Li, C. Qin, M. Shi, M. Ye, Layer-by-layer self-assembly of graphene nanoplatelets, Langmuir: ACS J. Surface. Colloid. 25 (2009) 6122–6128.
[47] G. Chen, Q.-F. Lü, H.-B. Zhao, SnO2-Decorated graphene/polyaniline nanocomposite for a high-performance supercapacitor electrode, J. Mater. Sci. Technol. 31 (2015) 1101–1107.
[48] G. Zhang, Z. Shao, W. Lu, F. Xie, X. Qin, B. Yi, Electrochemical preparation and characterization of PdPt nanocages with improved electrocatalytic activity toward oxygen reduction reaction, Electrochim. Acta 103 (2013) 66–76.
[49] S. Wang, L. Xu, H. Liang, et al., Self-interconnecting Pt nanowire network electrode for electrochemical amperometric biosensor, Nanoscale 7 (2015), 11460.
[50] D. Shuang, J. Xi, Y. Wu, et al., High loading MnO2, nanowires on graphene paper: facile electrochemical synthesis and use as flexible electrode for tracking hydrogen peroxide secretion in live cells, Anal. Chim. Acta 853 (2015) 200–206.
[51] J. Zhou, L. Tang, F. Yang, et al., MoS_2/Pt nanocomposite-functionalized microneedle for real-time monitoring of hydrogen peroxide release from living cells, Analyst 142 (2017).
[52] Q. Li, X. Qin, Y. Luo, et al., One-pot synthesis of Ag nanoparticles/reduced graphene oxide nanocomposites and their application for nonenzymatic H_2O_2, detection, Electrochim. Acta 83 (2012) 283–287.
[53] G. Nie, X. Lu, J. Lei, et al., Sacrificial template-assisted fabrication of palladium hollow nanocubes and their application in electrochemical detection toward hydrogen peroxide, Electrochim. Acta 99 (2013) 145–151.
[54] N. Zhang, J. Zheng, Synthesis of Ag–Fe2O3–RGO nanocomposites for the electrocatalytic reduction of H2O2, J. Mater. Sci. Mater. Electron. 28 (2017) 1–8.
[55] H. Ramezani, S. Azizi, S. Hosseini, NaY zeolite as a platform for preparation of Ag nanoparticles arrays in order to construction of H_2O_2 sensor, Sens. Actuators, B 248 (2017) 571–579.
[56] S. Rotsami, S. Azizi, S. Ghasemi, Using of silver nanoparticles incorporated in nanoporous ZSM-5 hierarchical zeolite prepared from bagasse as a new sensor for electrocatalytic determination of H2O2 in biological samples, J. Electroanal. Chem. 799 (2017) 583–594.
[57] Q. Chen, M.G. Espey, M.C. Krishna, J.B. Mitchell, C.P. Corpe, G.R. Buettner, E. Shacter, M. Levine, Pharmacologic ascorbic acid concentrations selectively kill cancer cells: action as a pro-drug to deliver hydrogen peroxide to tissues, Proc. Natl. Acad. Sci. U.S.A. 102 (2005) 13604–13609.
[58] Y. Zhang, et al., Graphene quantum dots/gold electrode and its application in living cell H2O2 detection, Nanoscale 5 (2013), 1816.
[59] H. Dai, W. Lü, X. Zuo, et al., A novel biosensor based on boronic acid functionalized metal-organic frameworks for the determination of hydrogen peroxide released from living cells, Biosens. Bioelectron. 95 (2017) 131–137.
[60] P. Wu, Y. Qian, P. Du, H. Zhang, C. Cai, Facile synthesis of nitrogen-doped graphene for measuring the releasing process of hydrogen peroxide from living cells, J. Mater. Chem. 22 (2012) 6402–6412.

Please cite this article in press as: Y. Fu, et al., Graphene blended with SnO_2 and Pd-Pt nanocages for sensitive non-enzymatic electrochemical detection of H_2O_2 released from living cells, Analytica Chimica Acta (2018), https://doi.org/10.1016/j.aca.2018.01.067